Ⓔ

A First-Layered Crustal Velocity Model for the Western Solomon Islands: Inversion of the Measured Group Velocity of Surface Waves Using Ambient Noise

by Chin-Shang Ku, Yu-Ting Kuo, Wei-An Chao, Shuei-Huei You, Bor-Shouh Huang, Yue-Gau Chen, Frederick W. Taylor, and Yih-Min Wu

ABSTRACT

Two earthquakes, M_w 8.1 in 2007 and M_w 7.1 in 2010, hit the western province of the Solomon Islands and caused extensive damage, which motivated us to establish a temporary seismic network around the rupture zones of these earthquakes. With the available continuous seismic data recorded from eight seismic stations, we cross correlate the vertical component of ambient-noise records and calculate Rayleigh-wave group velocity dispersion curves for interstation pairs. A genetic algorithm is adopted to fit the averaged dispersion curve and invert a 1D crustal velocity model, which constitutes two layers (upper and lower crust) and a half-space (uppermost mantle). The resulting thickness values for the upper and lower crust are 6.9 and 13.5 km, respectively. The shear-wave velocities (V_S) of the upper crust, lower crust, and uppermost mantle are 2.62, 3.54, and 4.10 km/s with V_P/V_S ratios of 1.745, 1.749, and 1.766, respectively. The differences between the predicted and observed travel times show that our 1D model (WSOLOCrust) has average 0.85- and 0.16-s improvements in travel-time residuals compared with the global iasp91 and local CRUST 1.0 models, respectively. This layered crustal velocity model for the western Solomon Islands can be further used as a referenced velocity model to locate earthquake and tremor sources as well as to perform 3D seismic tomography in this region.

Electronic Supplement: Figures showing the misfit of inversion process and the comparison between observed and synthetics and the location of experiments in previous studies and tables listing information about the seismic network, parameters of the genetic algorithm (GA), information of earthquakes used in this study, and results obtained from different 1D models.

INTRODUCTION

The Solomon Islands is located in the southwestern part of the Pacific Ocean. Several tectonic plates, including the Pacific, Australian, and Woodlark plates, subduct beneath the Solomon arc, forming an active subduction zone (Fig. 1). In 2007, an M_w 8.1 earthquake occurred in the western Solomon Islands and ruptured across the Pacific–Australian–Woodlark triple junction (Taylor *et al.*, 2008; Chen *et al.*, 2009; Miyagi *et al.*, 2009). This event generated a hazardous tsunami with a maximum wave height of 12 m that hit the western province of the Solomon Islands, which resulted in 52 deaths and thousands homeless (Fisher *et al.*, 2007; Fritz and Kalligeris, 2008). About 3 yrs later in 2010, a relatively small earthquake with the moment magnitude of 7.1 occurred near the hypocenter of the 2007 earthquake (Newman *et al.*, 2011; Kuo *et al.*, 2016). Despite its size, this event also generated a local tsunami (Newman *et al.*, 2011). Unfortunately, there is a lack of local seismic recording during these two earthquakes. Hence, neither analyzing the source mechanisms of the events in detail nor further developing the tsunami warning system is viable.

To understand the seismic activity in the western Solomon Islands, we installed eight broadband seismic stations around the rupture zone of the 2007 earthquake, aiming to provide quantities of records from earthquakes and continuous signals from ambient noise. The velocity structure of neighboring areas has been previously proposed (Cooper, Bruns, *et al.*, 1986; Cooper, Marlow, *et al.*, 1986; Miura, 1998; Shinohara *et al.*, 2003; Miura *et al.*, 2004; Yoneshima *et al.*, 2005); however, there is no available velocity model in our study area. Using a dense seismic network, an Earth structure model can be derived from either the travel-time tomography (e.g., Bording *et al.*, 1987) or the ambient-noise tomography (e.g., Shapiro

 doi: 10.1785/0220180126

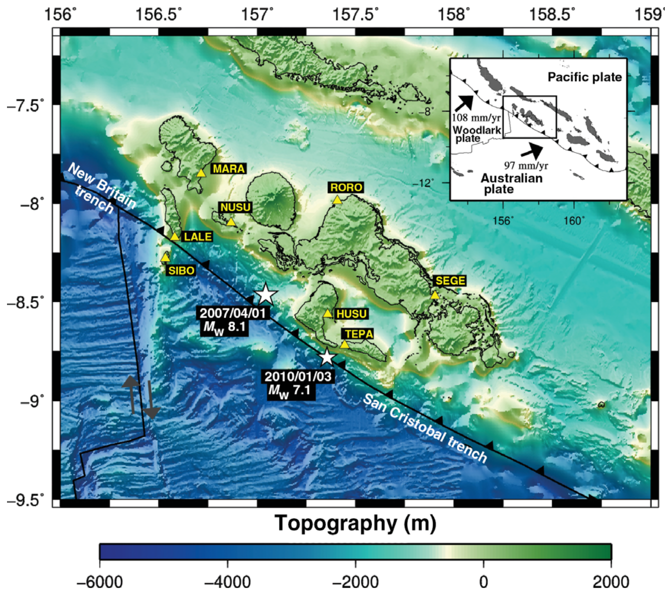

▲ **Figure 1.** The inset shows the plate tectonic setting around the Solomon Islands (black box represents our study area in the western Solomon Islands). The triple junction is located where the Pacific, Australian, and Woodlark plate boundaries intersect. The map displays the bathymetry and the distribution of seismic stations (yellow triangles). Two white stars indicate the epicenters of the earthquakes that occurred in 2007 and 2010, respectively.

et al., 2005; Lin *et al.*, 2007). Because of the large aperture of the station distribution and insufficient stations, we first study a simple 1D velocity structure. We accordingly conducted the genetic algorithm (GA; Holland, 1975) adopted for studying earthquake source mechanisms (e.g., Wu *et al.*, 2008; Chao *et al.*, 2011), to determine a 1D crustal velocity model by minimizing the misfit between observed data and the theoretical dispersion curves. We apply the Computer Programs in Seismology (CPS) package (Herrmann, 2013) to predict the theoretical dispersion curves. The observed dispersion curves herein are derived from the cross-correlograms after applying the multiple filter technique (MFT; Dziewonski *et al.*, 1969), and the averaged dispersion curve is used as the input data for an inversion algorithm. The reliability of the inversion scheme depends on the number of unknown parameters. So, we simplify the velocity model into two layers and a half space to provide a layered velocity model.

Because there is no previously published velocity model for the western Solomon Islands, our proposed 1D model is examined by a comparison with the global models iasp91 (Kennett and Engdahl, 1991) and CRUST 1.0 (Laske *et al.*, 2013). To check the deviation in between, the predicted travel time is computed by applying a Python package (Cake; Sebastian *et al.*, 2017) on different 1D models. We select earthquakes those occurred within our study area from the U.S. Geological Survey (USGS) earthquake catalog and pick the first arrival of each event manually to calculate the observed travel time. Thereby, the travel-time residuals between the observed and predicted travel times for each event can be estimated to verify the improvement of our 1D model. The advantage of this study using ambient noise and applying the GA to develop the velocity model is to avoid the trade-off between a velocity model and the hypocenter location. Our new 1D model can hence be a better-reference velocity model for seismic study and further help locate small local earthquakes. Walter *et al.* (2016) reported the evidence for triggering of tectonic tremor in the western Solomon Islands, indicating slow processes indeed happen in this area. To improve the searching for the triggered tremors, a reliable velocity model is urgently needed. Also, such a model will be essential for further understanding the tectonic details to help seismic hazard mitigation.

DATA PROCESSING AND GROUP VELOCITY MEASURMENTS

Based on the coverage of the rupture zone observed in the 2007 earthquake, we designed an eight-seismometer network and deployed the instruments in the western Solomon Islands since September 2009 (Fig. 1). The seismic instruments are equipped with the broadband seismometer (Trillium 120PA; Nanometrics Inc., Canada) and the 24-bits digital recorder (Q330S; Quanterra Inc., U.S.A.) with sampling rates of 100 Hz. In this study, the vertical-component continuous seismic data from eight broadband seismic stations are used. Records with time shifting or instrument problems are removed manually. The data lengths from the eight stations are shown in Ⓔ Table S1 (available in the electronic supplement to this article).

The empirical Green's function between two stations can be estimated from the ambient-noise cross-correlation function (CCF). In the past decades, the above statement has been verified by several studies (Campillo and Paul, 2003; Shapiro and Campillo, 2004; Snieder, 2004; Weaver and Lobkis, 2004; Stehly *et al.*, 2007). Based on the procedure of You *et al.* (2010), the data processing of continuous records can be summarized as follows: (1) preparing daily records of seismic data for each station; (2) removing the instrument response, mean, and linear trend; (3) applying a bandpass filter with a 2- to 50-s period range and decimating the sampling rate to 10 Hz; (4) conducting a one-bit normalization scheme (Larose *et al.*, 2004; Shapiro and Campillo, 2004); and (5) computing daily CCFs for each station pair with lag times ranging from −300 to 300 s. To increase the signal-to-noise ratio (SNR) of the CCFs, we stack all possible CCFs for each station pair to compute a stacked CCF (SCCF). Then the group velocity dispersion curves of each SCCF can be measured using the MFT (Dziewonski *et al.*, 1969). For more detailed information about the MFT used in this study, please refer to Corchete *et al.* (2007).

INVERSION SCHEME

Based on Darwin's natural evolution theory, the GA was proposed by Holland (1975) and has been approved as one of the powerful tools used to solve nonlinear problems. Many seismological studies adopted the GA to invert not only the crustal

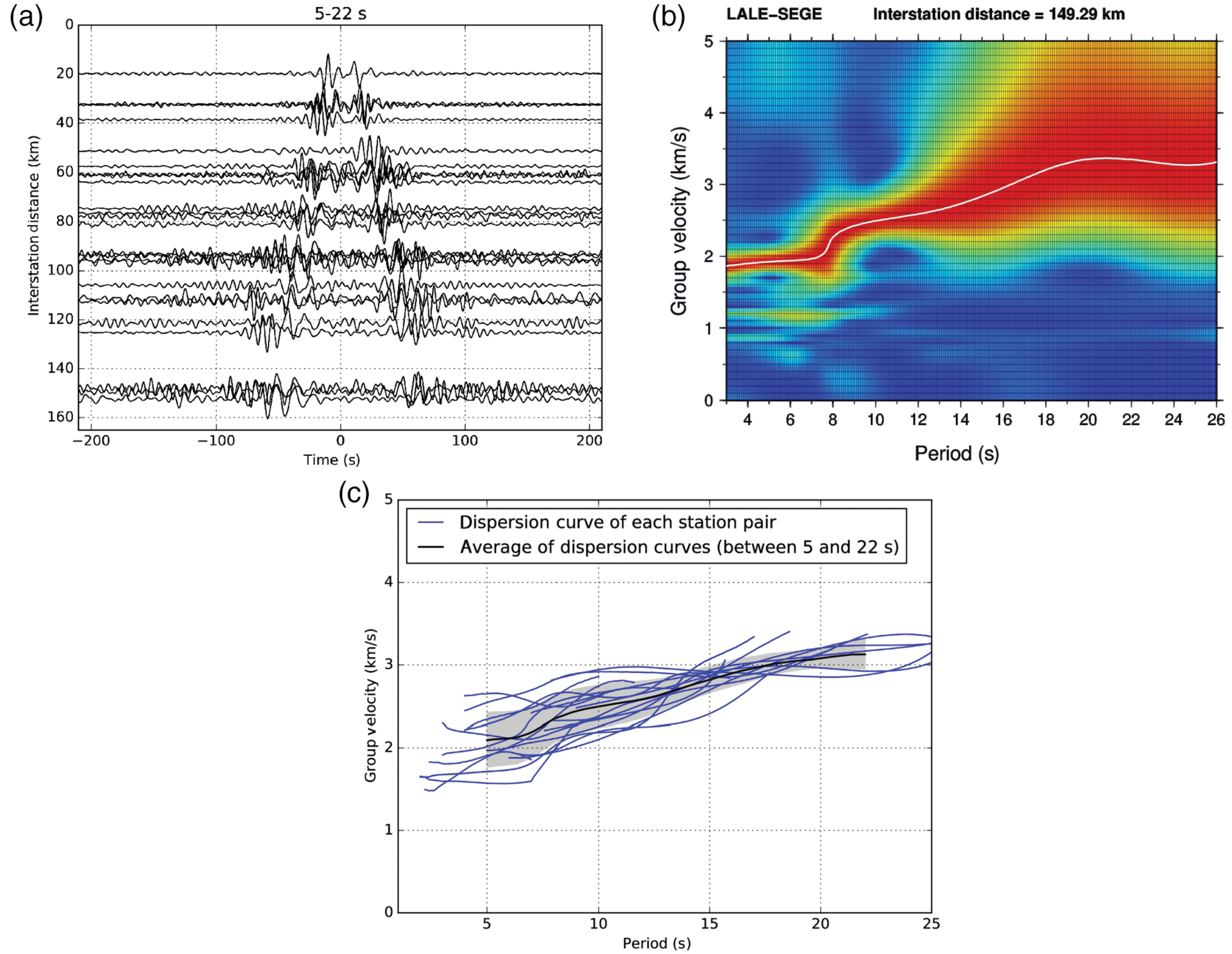

▲ **Figure 2.** (a) An example of cross-correlograms with different filtered periods. (b) An example of the result after applying multiple filter technique to one station pair (LALE-SEGE). The white line indicates the group velocity dispersion curve for this station pair. (c) Dispersion curves of each station pairs (blue lines). The black line indicates the averaged dispersion curve from period 5 to 22 s, which is used as input data for the genetic algorithm (GA) search. The gray part shows a range of one positive and one negative standard deviation.

velocity structure (Jin and Madariaga, 1993; Bhattacharyya *et al.*, 1999; Lopes and Assumpção, 2011) but also the source mechanism (Wu *et al.*, 2008; Chao *et al.*, 2011). To develop a velocity model consisting of two layers and a half space, we apply the GA to search for the best solution for the layer thickness V_S and V_P/V_S ratio that provides the minimum misfit between the observed and theoretical dispersion curves. Through an input-layered velocity model, we can apply the CPS (Herrmann, 2013) to calculate the theoretical group velocity dispersion curve. The thickness V_S and V_P/V_S ratio in each layer are randomly chosen (Ⓔ Table S2), and the density (ρ) of each layer is calculated by an empirical relation (Brocher, 2005):

$$\rho(\mathrm{g/cm^3}) = 1.6612V_P - 04721V_P^2 + 0.0671V_P^3 - 0.0043V_P^4 + 0.000106V_P^5. \quad (1)$$

We use the misfit between the observed and theoretical group velocity dispersion curves to evaluate the input model. The squared misfit in a given model (P) is defined as

$$S(P) = \sum[V_g^P(Ti) - V_g^{\mathrm{obs}}(Ti)]^2, \quad (2)$$

in which $V_g^P(Ti)$ and $V_g^{\mathrm{obs}}(Ti)$ are the theoretical and observed group velocity at period Ti, respectively.

In our GA search, 65 bits in total are used to present the crustal velocity structure parameters, different bits for different parameters to achieve a 0.01 km/s resolution in V_S, a 0.001 resolution in the V_P/V_S ratio, and a 0.1-km resolution in thickness (Ⓔ Table S2). Considering the efficiency of the computation, the population size in our GA is 30 for each generation. The working flow of our GA can be summarized as follows: (1) The initial populations are chosen randomly.

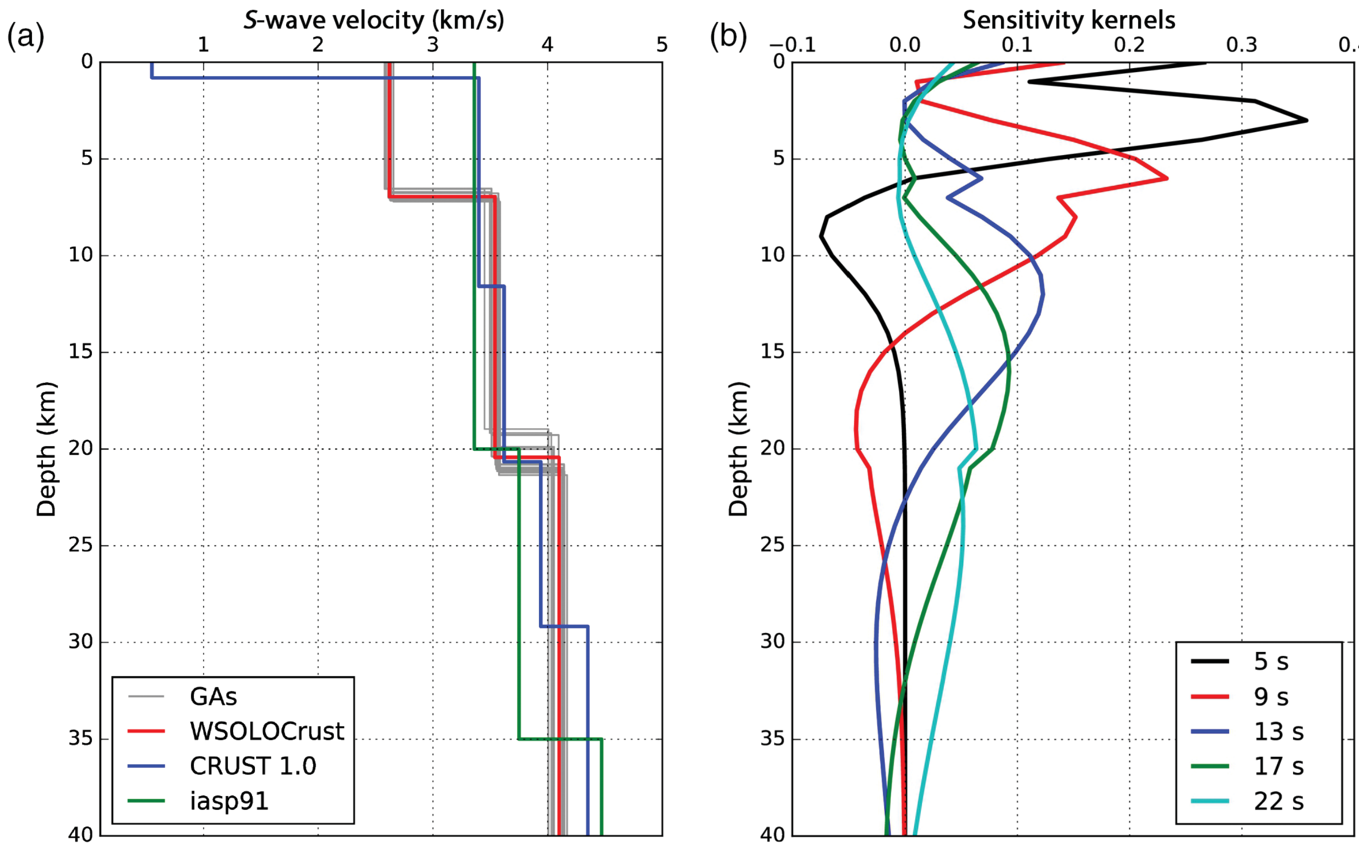

▲ **Figure 3.** (a) The *S*-wave (V_S) velocity model obtained from the GA. The gray line indicates the best model from each GA search. The red line shows the average 1D crustal velocity model and represents the WSOLOCrust model proposed by this study. Blue and green lines represent the local CRUST 1.0 and the global iasp91 velocity models, respectively. (b) Sensitivity kernels of Rayleigh-wave group velocity at selected periods are calculated with the WSOLOCrust model.

(2) Before going to the crossover operation, the models with higher fitness have higher probabilities of being selected as parents. (3) After parents are selected according to the fitness in the last generation, they go to the crossover operation with a certain probability (e.g., 95%), where parts of the parents' gene are combined to generate the next generation. A higher crossover probability leads to faster convergence (Goldberg, 1989), and a crossover probability of 90% is chosen in this study. (4) In addition to the crossover operation, the mutation operation can prevent the population evolution from converging to a local minimum of the misfit. The probability of mutation can optimally be set to $1/N$, in which N is the numbers of parameters in the GA search (Bäck, 1996). In this study, N is equal to 8 (Ⓔ Table S2), and a mutation probability of 12.5% is used. (5) The process is terminated after a certain number of generations through testing the different numbers between 50 and 1000; the results suggest that 600 generations yield a more efficient algorithm and an acceptable solution. Ⓔ Figure S1a shows an example of our GA result with running 1000 generations. In each generation, we can obtain the minimum value of misfit from 30 population results (Ⓔ Fig. S1a). The misfit does not decrease too much after the 500 generations. So, we select 600 generations this study. In total, we perform the GA search for 10 times (Ⓔ Fig. S1b shows the comparison between observed and synthetic dispersion curves) and then average the resulting velocity models to obtain our final 1D crustal velocity model.

RESULTS AND DISCUSSION

After stacking the daily CCFs to improve the SNR of the cross-correlograms for each station pair, Figure 2a shows an example that all the available SCCFs according to interstation distance. Data in Figure 2a were bandpass filtered between 5 and 22 s. The last step before measuring the dispersion curves is that the cross-correlograms are symmetrized and turned into one-side signals by averaging the causal and the acausal parts. This method of symmetrization was applied in most previous studies (e.g., Yao *et al.*, 2006; You *et al.*, 2010). Based on the MFT procedure (Dziewonski *et al.*, 1969; Corchete *et al.* 2007), the group velocity dispersion curves can be directly estimated. An example of the group velocity dispersion curve of one station pair derived from the MFT is shown in Figure 2b. Bensen *et al.* (2007) suggest that a reliable dispersion measurement at period required an interstation distance at least three times the wavelength, but alternative techniques also be tested in recent studies, for example, two-wavelength criteria (Lin *et al.*, 2009; Porritt *et al.*, 2011; Mordret *et al.*, 2013) or one-wavelength criteria (Luo *et al.*, 2015; Wang *et al.*, 2016). To include more observation data, we adopted one-wavelength criteria in this study. Figure 2c shows the averaged dispersion curve (black line) and all available SCCFs (blue lines) that satisfied one-wavelength criteria (Luo *et al.*, 2015; Wang *et al.*, 2016). The averaged dispersion curve at the selected period range (5–22 s) is as the input data for the inversion scheme.

By adopting 600 generations and a randomly created model of the first generation for the GA searching, a 1D velocity model (gray line in Fig. 3a) can be determined by minimizing the misfit between the observed and predicted dispersion curves. To test the stability of the GA, we further perform the GA 10 times and determine the final model (red line in Fig. 3a) by averaging all resulting 1D velocity models. The WSOLOCrust model is used to represent the averaged model hereafter. WSOLOCrust model exhibits a Moho depth of 20.4 ± 1.5 km and a thickness for the upper crust of 6.9 ± 0.4 km. The V_S values and corresponding V_P/V_S ratios of the upper crust, the lower crust, and the uppermost mantle are 2.62 ± 0.04, 3.54 ± 0.14, and 4.10 ± 0.10 km/s and 1.745, 1.749, and 1.766, respectively (Fig. 3a). Figure 3b shows the sensitivity kernels of WSOLOCrust model. Sensitivity is defined as the variation in group velocity caused by a small variation in V_S at a given depth. The different selected period sensitive to different depths (e.g., the period at 22 s has the peak sensitivity to the subsurface structure at about 20 km depth).

A series of marine seismic refraction traverses have been carried out in the Solomon Islands by members of the Hawaii Institute of Geophysics (Furumoto *et al.*, 1970). In 1994, five ocean-bottom seismometers (OBSs) were deployed around the Russell Islands (Ⓔ Fig. S2) to investigate microearthquake seismicity (Shinohara *et al.*, 2003). Yoneshima *et al.* (2005) deployed 40-day OBSs in 1998 to detect the microseismic activity near the Shortland basin of the Solomon Islands (Ⓔ Fig. S2) and proposed a velocity structure to minimize the residuals of the travel time within their OBS seismic network. Both of those studies presented information on the crustal structure near the western Solomon Islands, but their study areas were not exactly the same as this study (Ⓔ Fig. S2). Thus, we select the global models iasp91 (Kennett and Engdahl, 1991) and CRUST 1.0 (Laske *et al.*, 2013) to compare with WSOLOCrust model. CRUST 1.0 is a global 3D crustal velocity model with 1° × 1° resolution. Here, we select 8.25° S and 157.25° E for an input point (Ⓔ Fig. S2) to extract a point crustal velocity model as a local model that consists of four layers above the mantle, including sediment, upper crust, middle crust, and lower crust (blue line in Fig. 3a). The most significant difference between the WSOLOCrust model and other models is in the shallow part (Fig. 3a). The V_S (~2.62 km/s) of the upper crust in WSOLOCrust model is obviously lower than those in other models (~3.4 km/s). The Moho depth (~20.4 km) for the WSOLOCrust model is also shallower than those for other models. (The Moho depths for iasp91 and CRUST 1.0 are ~35 and 29 km, respectively.)

Furumoto *et al.* (1970) used gravity anomalies and seismic refraction to estimate the crustal thickness, and several points (A, A*, P, and F in Ⓔ Fig. S2) in their experiment are close to our study area. Their reported mantle depths for points A, A*, P, and F are 26.7, 25.0, 14.7, and 7.8 km, respectively. Shinohara *et al.* (2003) used a simple 1D velocity model for the hypocenter location, which was simulated by the results of previous refraction studies (Cooper, Bruns, *et al.*, 1986; Cooper, Marlow, *et al.*, 1986; Miura, 1998; Miura *et al.*, 2004), and the Moho depth was ~30 km in their model. Yoneshima *et al.* (2005) modeled a Moho depth of ~25 km. The Moho depth presented in this study is ~20.4 km. The differences of Moho depths probably imply structural heterogeneity around the study area. More studies, such as the receiver functions method using data from our seismic network, are necessary to reconfirm the hypothesis.

To test the capability of the WSOLOCrust model, we constructed a procedure to investigate the influences of the velocity structure. First, we selected seismic data for local earthquakes from the USGS earthquake catalog by the following criteria: (1) moment magnitude (M_w) is larger than 5 that with better horizontal location constraint from a global earthquake catalog. (2) The event is recorded by at least three stations in our local network. We selected 54 events in total from September 2009 to 2016 and summarized the information about the events (Ⓔ Table S3). Second, we manually picked the first arrival time (FAT) for each event and adopted the original time (OT) from the USGS catalog to calculate the observed travel time (OTT = FAT − OT) for each station. Third, we applied a Python package called Cake to calculate the predicted travel time (PTT) of each station. Cake is a part of Pyrocko (Sebastian *et al.*, 2017), which is an open-source seismology toolbox and library. Pyrocko can be used to process geophysical and seismological data. Cake can be used to solve classical seismic ray theory problems for a layered model. Cake also allows us to apply on different-layered velocity models. To emphasize the apparent differences in the shallow parts of the velocity models, in the deep part (below the depth 77.5 km), we adopt the same structure in the iasp91 model, in the CRUST 1.0 model, and in the WSOLOCrust model. We hence apply Cake to the 1D model to calculate the root mean square (rms) values of the travel-time residuals for each event. We can consequently estimate the average rms values for different velocity models (Fig. 4):

$$\mathrm{rms}_i = \sqrt{\frac{\sum_{j=1}^{n}(\mathrm{PTT}_j - \mathrm{OTT}_j)^2}{n}}, \tag{3}$$

$$\mathrm{Avg.rms} = \frac{\sum_{i=1}^{k}\mathrm{rms}_i}{k}, \tag{4}$$

in which PTT_j and OTT_j are the predicted and observed travel times for the jth station during the ith event, respectively; n is the number of stations that recorded the ith event; and k is 54 indicates the number of events that we used in this study. Ⓔ Table S3 also shows the rms values obtained from different velocity models during each event. From Figure 4, it is evident

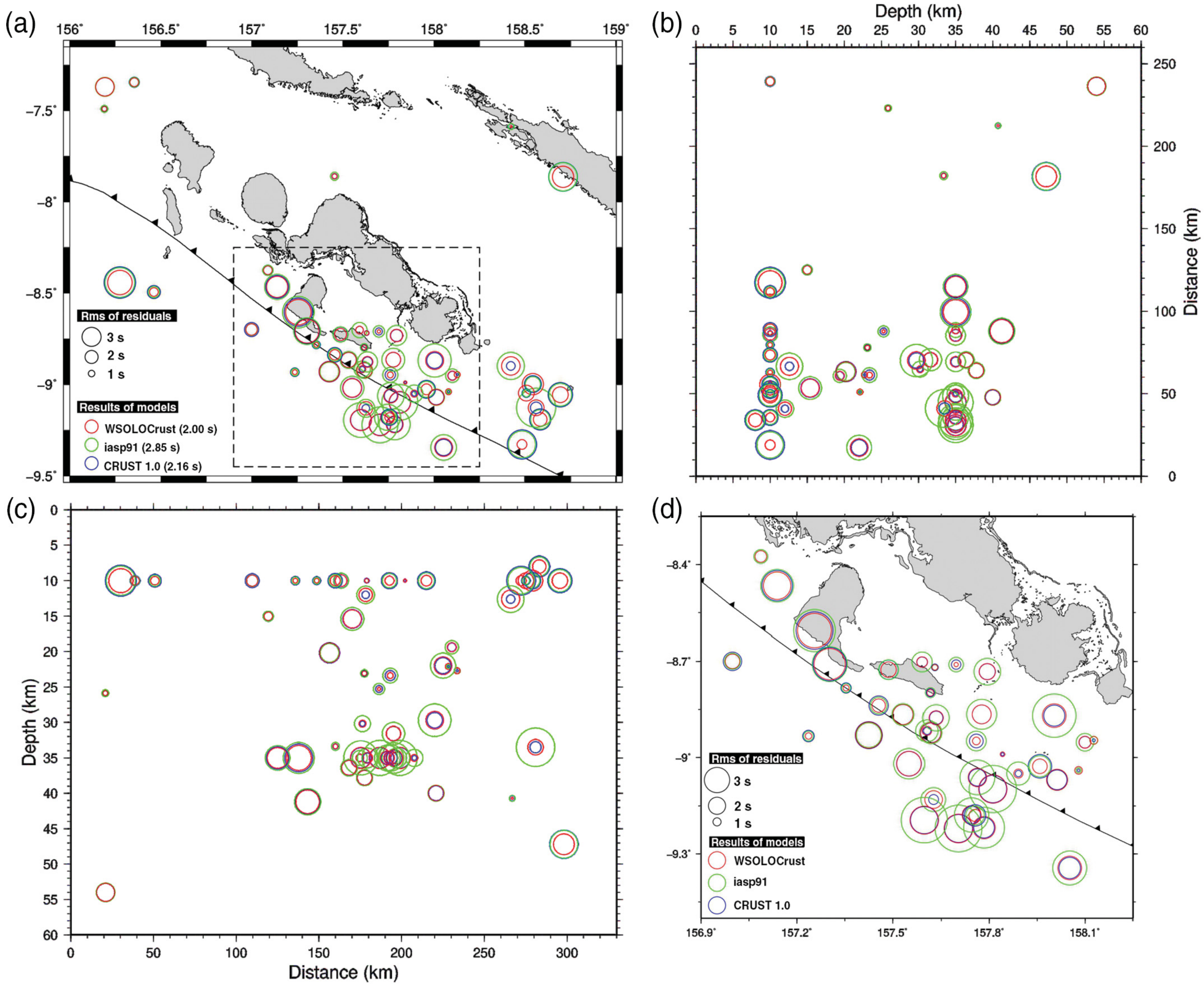

▲ **Figure 4.** (a) The open circles indicate the epicenters of earthquakes (Ⓔ Table S3, available in the electronic supplement to this article). The size of the circle shows the root mean square (rms) of residuals (in seconds) obtained from the difference between the observed and predicted travel times. In this figure, different models are applied to calculate the travel time of the first-arrival phase in each event. The different colors represent the rms of residuals from different models. (b) and (c) are the same as (a) but show the north–south and the west–east sections, respectively. (d) The results are displayed within the dashed line of (a).

that the WSOLOCrust model improves the travel-time residuals compared with the global iasp91 model. It is also better than the local model extracted from the CRUST 1.0 model. Figures 4b and 4c show results of the north–south and the west–east sections, respectively. Figure 5 shows the distributions of improvements of rms for each event. We calculate the improvement by subtracting the minimum rms value from the second smallest rms value among three 1D velocity models. The size of the circle shows improvement of rms value, and color indicates the model that derives the minimum rms value. Obviously, the WSOLOCrust model derives the minimum rms of residuals around our seismic array (yellow triangles in Fig. 5a). From Figure 5b,c, the WSOLOCrust model presents smaller rms of residuals on the earthquakes that occurred at the shallower depth (around depth 10 km) than other velocity models. It also shows that WSOLOCrust model has a better improvement in the shallow structure. But there are still 22 events of 54 and 4 events of 54 in which the CRUST 1.0 and iasp91 models can yield smaller rms values, respectively. Especially for events at the depth around 30–35 km, the WSOLOCrust model derived relatively higher rms of time residuals. These events are located outside of our seismic array. We suggest that the frequency band used in the cross correlations may limit resolving velocity structures below 30 km, and array aperture also limits our results. However, the improvements obtained from other two models are smaller compared with the WSOLOCrust model. The

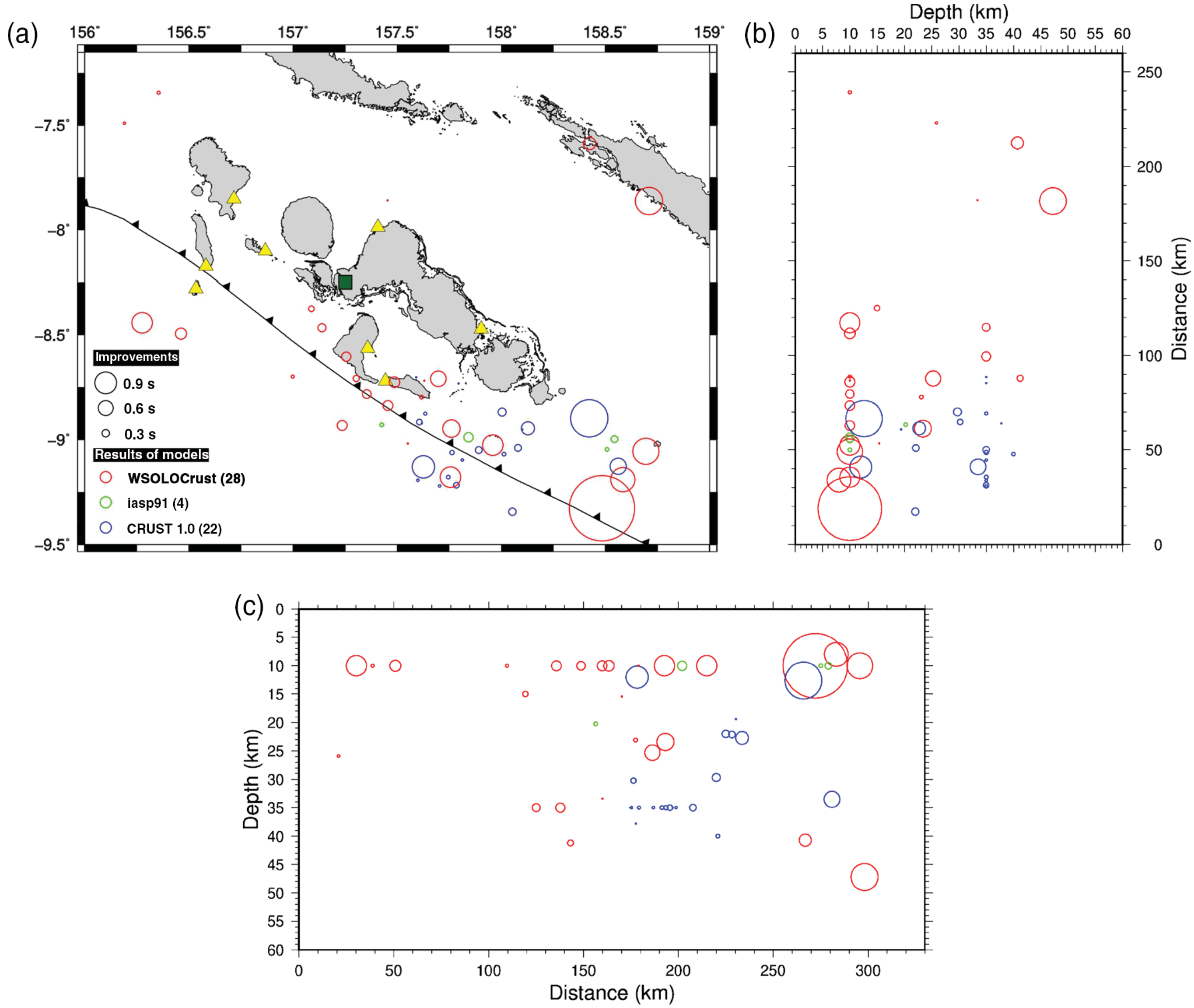

▲ **Figure 5.** (a) Improvements of each event by subtracting the minimum rms value from the second smallest rms value among three 1D velocity models. For each event, we use the model that derives the minimum rms value to represent it. The red, green, and blue color mean WSOLOCrust, iasp91, and CRUST 1.0, respectively. The number in parentheses means how many events estimate the minimum rms through this model. Yellow triangles indicate the seismic stations that we used to calculate the travel-time residuals. The green square means the point that we apply to extract a point crustal velocity model form CRUST 1.0. (b) and (c) are the same as (a) but show the north–south and the west–east sections, respectively.

WSOLOCrust model gives the smallest averaged rms of residuals of all events (Fig. 4a). The WSOLOCrust model emerges as a better reference velocity model than others.

The WSOLOCrust crustal velocity model is obtained from the average group velocity dispersion curves of different station pairs. This process may not adequately represent the crustal structure beneath the whole region. However, by comparing the travel-time residuals for the different 1D models, the WSOLOCrust model has better performance than the iasp91 model as well as the CRUST 1.0 model. The next phase of our cooperative project plan will install a dense OBS array in the western Solomon Islands. The WSOLOCrust model will play an important role in providing initial information to invert a 2D or 3D model.

CONCLUSIONS

In this study, we recover the Rayleigh wave from vertical-component recordings. The group velocity dispersion curves of the Rayleigh wave are determined from the cross correlation of ambient noise. The average dispersion curve between 5 and 22 s is taken as the observed to compare with the theoretical dispersion curve. Finally, we apply the GA to search model space efficiently to obtain a 1D crustal velocity model, WSOLOCrust, which is the first-layered crustal velocity model in the western Solomon Islands. V_S for the upper crust, lower crust, and uppermost mantle are 2.62, 3.54, and 4.10 km/s, respectively, and the relative V_P/V_S ratios are 1.745, 1.749, and 1.766, respectively. The depth to the Moho is 20.4 km, and the thicknesses of the upper crust and lower crust are 6.9 and 13.5 km, respectively. By comparing the travel-time residuals for 54 local events, the averaged rms value of travel-time residuals from WSOLOCrust model is better than that of the iasp91 and CRUST 1.0 models. The WSOLOCrust model has average 0.85- and 0.16-s improvements compared with the iasp91 and CRUST 1.0 models, respectively.

The Solomon Island is in the area with a very complicated tectonic structure. The 1D velocity model may not satisfy for all of the seismological purposes. Thus, a detailed 2D or 3D velocity model could be achieved by deploying a dense OBS array in the next phase of our cooperative project. The layered crustal velocity model for the western Solomon Islands proposed in this study will provide a good-reference velocity model. It will be constructive for future research in the Solomon Island.

DATA AND RESOURCES

The data used in this study were obtained from the Institute of Earth Sciences (IES) of Academia Sinica and the National Taiwan University (NTU). For data requests, please contact the author C.-S. Ku (backnew@earth.sinica.edu.tw). The U.S. Geological Survey (USGS) global earthquake catalog is maintained at https://earthquake.usgs.gov/earthquakes/search (last accessed April 2018). The Computer Programs in Seismology (CPS) is available at http://www.eas.slu.edu/eqc/eqccps.html (last accessed April 2018). Seismic Analysis Code (SAC) is available at http://ds.iris.edu/files/sac-manual (last accessed April 2018). Pyrocko (software for seismology) is available at https://pyrocko.org (last accessed April 2018).

ACKNOWLEDGMENTS

This research was supported by the Ministry of Science and Technology (MOST) of Taiwan (MOST-105-2116-M-002-030-MY3, MOST-105-2116-M-001-025-MY3, and MOST-106-2116-M-002-019-MY3). The instruments used in this study provided by the Taiwan Earthquake Research Center Instrument Pool (TECIP) and the Institute of Earth Sciences (IES), Academia Sinica, Taiwan. The authors are grateful to the Embassy of the Republic of China (Taiwan) in the Solomon Islands; the Seismology Section of the Ministry of Mines, Energy, and Rural Electrification of the Solomon Islands; and the Kolombangara Forest Products Limited for the support in the western province. The authors thank Herrmann (2013) for Computer Programs in Seismology (CPS) and Sebastian *et al.* (2017) for Pyrocko software that were used in data processing, Wessel and Smith (1998) for the Generic Mapping Tool (GMT) software, and Hunter (2007) for the Matplotlib software that were used in plotting figures. The authors thank Y. C. Lai, T. C. Chi, and W. G. Huang for their comments and discussion. They also thank Alison K. Papabatu, James Tsai, and Richard Lo for their help with fieldwork.

REFERENCES

Bäck, T. (1996). *Evolutionary Algorithms in Theory and Practice*, Oxford University Press, New York, New York.

Bensen, G. D., M. H. Ritzwoller, M. P. Barmin, A. L. Levshin, F. Lin, M. P. Moschetti, N. M. Shapiro, and Y. Yang (2007). Processing seismic ambient noise data to obtain reliable broad-band surface wave dispersion measurements, *Geophys. J. Int.* **169,** 1239–1260, doi: 10.1111/j.1365-246X.2007.03374.x.

Bhattacharyya, J., A. F. Sheehan, K. Tiampo, and J. Rundle (1999). Using a genetic algorithm to model broadband regional waveforms for crustal structure in the western United States, *Bull. Seismol. Soc. Am.* **89,** 202–214.

Bording, R. P., A. Gersztenkom, L. R. Lines, J. A. Scales, and S. Treitel (1987). Application of seismic travel-time tomography, *Geophys. J. Int.* **90,** 285–303.

Brocher, T. M. (2005). Empirical relations between elastic wavespeeds and density in the Earth's crust, *Bull. Seismol. Soc. Am.* **95,** 2081–2092, doi: 10.1785/0120050077.

Campillo, M., and A. Paul (2003). Long-range correlations in the diffuse seismic coda, *Science* **299,** 547–549, doi: 10.1126/science.1078551.

Chao, W. A., L. Zhao, and Y. M. Wu (2011). Centroid fault-plane inversion in the three-dimensional velocity structure using strong-motion records, *Bull. Seismol. Soc. Am.* **101,** 1330–1340, doi: 10.1785/0120100245.

Chen, T., A. V. Newman, L. Feng, and H. M. Fritz (2009). Slip distribution from the 1 April 2007 Solomon Islands earthquake: A unique image of near-trench rupture, *Geophys. Res. Lett.* **36,** 6–11, doi: 10.1029/2009GL039496.

Cooper, A. K., T. R. Bruns, and R. A. Wood (1986). Shallow crustal structure of the Solomon Islands intra-arc basin from sonobouy seismic studies, in *Geology and Offshore Resources of Pacific Islands Arcs—Central and Western Solomon Islands*, Vol. 4**,** Circum-Pacific Council for Energy and Mineral Resources, Houston, Texas, 135–156.

Cooper, A. K., M. S. Marlow, and R. A. Wood (1986). Deep structure of the central and southern Solomon region: implications for tectonic origin, in *Geology and Offshore Resources of Pacific Islands Arcs—Central and Western Solomon Islands*, Vol. 4**,** Circum-Pacific Council for Energy and Mineral Resources, Houston, Texas, 157–175.

Corchete, V., M. Chourak, and H. M. Hussein (2007). Shear wave velocity structure of the Sinai Peninsula from Rayleigh wave analysis, *Surv. Geophys.* **28,** 299–324, doi: 10.1007/s10712-007-9027-6.

Dziewonski, A., S. Bloch, and M. Landisman (1969). A technique for the analysis of transient seismic signals, *Bull. Seismol. Soc. Am.* **59,** 427–444.

Fisher, M. A., E. L. Geist, R. Sliter, F. L. Wong, C. Reiss, and D. M. Mann (2007). Preliminary analysis of the earthquake (M_w 8.1) and tsunami of April 1, 2007, in the Solomon Islands, southwestern Pacific Ocean, *Sci. Tsunami Hazards* **26,** 3–20.

Fritz, H. M., and N. Kalligeris (2008). Ancestral heritage saves tribes during 1 April 2007 Solomon Islands tsunami, *Geophys. Res. Lett.* **35,** L01607, doi: 10.1029/2007GL031654.

Furumoto, A. S., D. M. Hussong, J. F. Campbell, G. H. Sutton, A. Malahoff, J. C. Rose, and G. P. Woollard (1970). Crustal and upper mantle structure of the Solomon Islands as revealed by seismic refraction survey of November–December 1966, *Pac. Sci.* **24,** 315–332.

Goldberg, D. E. (1989). *Genetic Algorithms in Search, Optimization, and Machine Learning*, Addison Wesley, Reading, Massachusetts.

Herrmann, R. B. (2013). Computer programs in seismology: An evolving tool for instruction and research, *Seismol. Res. Lett.* **84,** 1081–1088, doi: 10.1785/0220110096.

Holland, J. H. (1975). *Adaptation in Natural and Artificial Systems*, University of Michigan Press, Ann Arbor, Michigan.
Hunter, J. D. (2007). Matplotlib: A 2D graphics environment, *IEEE Comput. Soc.* **9,** 90–95, doi: 10.1109/MCSE.2007.55.
Jin, S., and R. Madariaga (1993). Background velocity inversion with a genetic algorithm, *Geophys. Res. Lett.* **20,** 93–96, doi: 10.1029/92GL02781.
Kennett, B. L. N., and E. R. Engdahl (1991). Travel times for global earthquake location and phase association, *Geophys. J. Int.* **105,** 429–465, doi: 10.1111/j.1365-246X.1991.tb06724.x.
Kuo, Y. T., C. S. Ku, Y. G. Chen, Y. Wang, Y. N. N. Lin, R. Y. Chuang, Y. J. Hsu, F. W. Taylor, B. S. Huang, and H. Tung (2016). Characteristics on fault coupling along the Solomon megathrust based on GPS observations from 2011 to 2014, *Geophys. Res. Lett.* **43,** 8519–8526, doi: 10.1002/2016GL070188.
Larose, E., A. Derode, M. Campillo, and M. Fink (2004). Imaging from one-bit correlations of wideband diffuse wave fields, *J. Appl. Phys.* **95,** 8393–8399, doi: 10.1063/1.1739529.
Laske, G., G. Masters, Z. Ma, and M. Pasyanos (2013). Update on CRUST 1.0: A 1-degree global model of Earth's crust, *Geophys. Res. Abstr.* **15,** EGU2013–2658.
Lin, F. C., M. H. Ritzwoller, and R. Snieder (2009). Eikonal tomography: Surface wave tomography by phase front tracking across a regional broad-band seismic array, *Geophys. J. Int.* **177,** 1091–1110, doi: 10.1111/j.1365-246X.2009.04105.x.
Lin, F. C., M. H. Ritzwoller, J. Townend, S. Bannister, and M. K. Savage (2007). Ambient noise Rayleigh wave tomography of New Zealand, *Geophys. J. Int.* **170,** 649–666, doi: 10.1111/j.1365-246X.2007.03414.x.
Lopes, A. E. V., and M. Assumpção (2011). Genetic algorithm inversion of the average 1D crustal structure using local and regional earthquakes, *Comput. Geosci.* **37,** no. 9, 1372–1380, doi: 10.1016/j.cageo.2010.11.006.
Luo, Y., Y. Yang, Y. Xu, H. Xu, K. Zhao, and K. Wang (2015). On the limitations of interstation distances in ambient noise tomography, *Geophys. J. Int.* **201,** 652–661, doi: 10.1093/gji/ggv043.
Miura, S. (1998). Seismic velocity structure of the Solomon double trench-island arc system using airgun array and ocean bottom seismometers, *Ph.D. Thesis*, Chiba University, Chiba, Japan, 113 pp. (in Japanese).
Miura, S., K. Suyehiro, S. Shinohara, N. Takahashi, E. Araki, and A. Taira (2004). Seismological structure and implications of collision of Ontong Java plateau and Solomon Island arc from ocean bottom seismometer–airgun data, *Tectonophysics* **389,** 191–220, doi: 10.1016/j.tecto.2003.09.029.
Miyagi, Y., T. Ozawa, and M. Shimada (2009). Crustal deformation associated with an M 8.1 earthquake in the Solomon Islands, detected by ALOS/PALSAR, *Earth Planet. Sci. Lett.* **287,** 385–391, doi: 10.1016/j.epsl.2009.08.022.
Mordret, A., N. M. Shapiro, S. S. Singh, P. Roux, and O. Barkved (2013). Helmholtz tomography of ambient noise surface wave data to estimate Scholte wave phase velocity at Valhall Life of the Field, *Geophysics* **78,** no. 2, WA99–WA109, doi: 10.1190/GEO2012-0303.1.
Newman, A. V., L. Feng, H. M. Fritz, Z. M. Lifton, N. Kalligeris, and Y. Wei (2011). The energetic 2010 M_w 7.1 Solomon Islands tsunami earthquake, *Geophys. J. Int.* **186,** 775–781, doi: 10.1111/j.1365-246X.2011.05057.x.
Porritt, R. W., R. M. Allen, D. C. Boyarko, and M. R. Brudzinski (2011). Investigation of Cascadia segmentation with ambient noise tomography, *Earth Planet. Sci. Lett.* **309,** 67–76, doi: 10.1016/j.epsl.2011.06.026.
Sebastian, H., K. Marius, I. Marius, C. Simone, D. Simon, G. Francesco, J. Carina, M. Tobias, N. Numa, S. Andreas, *et al.* (2017). Pyrocko—An open source seismology toolbox and library, v.0.3, *GFZ Data Services*, doi: 10.5880/GFZ.2.1.2017.001.
Shapiro, N. M., and M. Campillo (2004). Emergence of broadband Rayleigh waves from correlations of the ambient seismic noise, *Geophys. Res. Lett.* **31,** 8–11, doi: 10.1029/2004GL019491.
Shapiro, N. M., M. Campillo, L. Stehly, and M. H. Ritzwoller (2005). High-resolution surface wave tomography from ambient seismic noise, *Science* **307,** 1615–1618, doi: 10.1126/science.1108339.
Shinohara, M., K. Suyehiro, and T. Murayama (2003). Microearthquake seismicity in relation to double convergence around the Solomon Islands arc by ocean-bottom seismometer observation, *Geophys. J. Int.* **153,** 691–698, doi: 10.1046/j.1365-246X.2003.01940.x.
Snieder, R. (2004). Extracting the Green's function from the correlation of coda waves: A derivation based on stationary phase, *Phys. Rev.* **69,** 046610, doi: 10.1103/PhysRevE.69.046610.
Stehly, L., M. Campillo, and N. M. Shapiro (2007). Traveltime measurements from noise correlation: Stability and detection of instrumental time-shifts, *Geophys. J. Int.* **171,** 223–230, doi: 10.1111/j.1365-246X.2007.03492.x.
Taylor, F. W., R. W. Briggs, C. Frohlich, A. Brown, M. Hornbach, A. K. Papabatu, A. J. Meltzner, and D. Billy (2008). Rupture across arc segment and plate boundaries in the 1 April 2007 Solomons earthquake, *Nature Geosci.* **1,** 253–257, doi: 10.1038/ngeo159.
Walter, J., L. M. Wallace, F. W. Taylor, C. S. Ku, Y. T. Kuo, M. G. Bevis, E. C. Kendrick, A. K. Papabatu, T. Toba, B. S. Huang, *et al.* (2016). Triggered tremor and slow slip in the western Solomon Islands, *AGU Chapman Conf. on the Slow Slip Phenomena M-25*, Ixtapa, Guerrero, Mexico, 21–25 February 2016.
Wang, Y., F. C. Lin, B. Schmandt, and J. Farrell (2016). Ambient noise tomography across Mount St. Helens using a dense seismicity, *J. Geophys. Res.* **122,** 4492–4508, doi: 10.1002/2016JB013769.
Weaver, R. L., and O. I. Lobkis (2004). Diffuse fields in open systems and the emergence of the Green's function, *J. Acoust. Soc. Am.* **116,** 2731–2734, doi: 10.1121/1.1810232.
Wessel, P., and W. H. F. Smith (1998). New, improved version of Generic Mapping Tools released, *Eos Trans. AGU* **79,** 579.
Wu, Y. M., L. Zhao, C. H. Chang, and Y. J. Hsu (2008). Focal mechanism determination in Taiwan by genetic algorithm, *Bull. Seismol. Soc. Am.* **98,** 651–661, doi: 10.1785/0120070115.
Yao, H., R. D. Van Der Hilst, and M. V. De Hoop (2006). Surface-wave array tomography in SE Tibet from ambient seismic noise and two-station analysis—I. Phase velocity maps, *Geophys. J. Int.* **166,** 732–744, doi: 10.1111/j.1365-246X.2006.03028.x.
Yoneshima, S., K. Mochizuki, E. Araki, R. Hino, M. Shinohara, and K. Suyehiro (2005). Subduction of the Woodlark basin at the New Britain trench, Solomon Islands region, *Tectonophysics* **397,** 225–239, doi: 10.1016/j.tecto.2004.12.008.
You, S. H., Y. Gung, L. Y. Chiao, Y. N. Chen, C. H. Lin, W. T. Liang, and Y. L. Chen (2010). Multiscale ambient noise tomography of short-period Rayleigh waves across northern Taiwan, *Bull. Seismol. Soc. Am.* **100,** 3165–3173, doi: 10.1785/0120090394.

Chin-Shang Ku[1]
Yue-Gau Chen
Yih-Min Wu[1,2]
Department of Geosciences
National Taiwan University
Number 1, Section 4, Roosevelt Road
Taipei 10617, Taiwan
backnew@earth.sinica.edu.tw
ygchen@ntu.edu.tw
drymwu@ntu.edu.tw

Yu-Ting Kuo
Bor-Shouh Huang
Institute of Earth Sciences
Academia Sinica
Number 128, Section 2, Academia Road
Taipei 11529, Taiwan
yutingkuo@earth.sinica.edu.tw
hwbs@earth.sinica.edu.tw

Wei-An Chao
Department of Civil Engineering
National Chiao Tung University
Number 1001, University Road
Hsinchu 30010, Taiwan
vvnchao@gmail.com

Shuei-Huei You
Ship and Ocean Industries R&D Center
Ministry of Economic Affairs
14F., Number 27, Section 2, Zhongzheng E. Road
Tamsui, New Taipei City 25170, Taiwan
wateryou@mail.soic.org.tw

Frederick W. Taylor
Institute for Geophysics
Jackson School of Geosciences
University of Texas at Austin
J.J. Pickle Research Campus, Building 196
10100 Burnet Road (R2200)
Austin, Texas 78758-4445 U.S.A.
fred@ig.utexas.edu

Published Online 26 September 2018

[1] Also at Institute of Earth Sciences, Academia Sinica, 128 Sinica Road Section 2, Taipei 15529, Taiwan; yihmin.wu@gmail.com.
[2] Also at NTU Research Center for Future Earth, National Taiwan University, Number 1, Section 4, Roosevelt Road, Taipei 10617, Taiwan.